RELIC GRAVITATIONAL WAVES FROM THE CHIRAL MAGNETIC EFFECT

Axel Brandenburg[1,2,3,4], Yutong He[1,2], Tina Kahniashvili[3,4,5], Matthias Rheinhardt[6], and Jennifer Schober[7]
[1]Nordita, KTH Royal Institute of Technology and Stockholm University, Hannes Alfvéns väg 11, SE-10691 Stockholm, Sweden
[2]Department of Astronomy, AlbaNova University Center, Stockholm University, SE-10691 Stockholm, Sweden
[3]McWilliams Center for Cosmology and Department of Physics, Carnegie Mellon University, 5000 Forbes Ave, Pittsburgh, PA 15213, USA
[4]Faculty of Natural Sciences and Medicine, Ilia State University, 3-5 Cholokashvili St., 0194 Tbilisi, Georgia
[5]Department of Physics, Laurentian University, Ramsey Lake Road, Sudbury, ON P3E 2C, Canada
[6]Department of Computer Science, Aalto University, PO Box 15400, FI-00076 Aalto, Finland
[7]Laboratoire d'Astrophysique, EPFL, CH-1290 Sauverny, Switzerland

January 21, 2021, Revision: 1.221

Chiral MHD

$$\frac{\partial \boldsymbol{B}}{\partial t} = \boldsymbol{\nabla} \times [\boldsymbol{u} \times \boldsymbol{B} + \eta(\mu_5 \boldsymbol{B} - \boldsymbol{J})], \quad \boldsymbol{J} = \boldsymbol{\nabla} \times \boldsymbol{B},$$

$$\frac{\mathrm{D}\mu_5}{\mathrm{D}t} = -\lambda\,\eta\,(\mu_5 \boldsymbol{B} - \boldsymbol{J}) \cdot \boldsymbol{B} + D_5 \nabla^2 \mu_5 - \Gamma_{\mathrm{f}} \mu_5,$$

Chiral chemical potential

$$\mu_5 = 24\,\alpha_{\mathrm{em}}\,(n_{\mathrm{L}} - n_{\mathrm{R}})\,(\hbar c / k_{\mathrm{B}} T)^2,$$

Relativistic EoS

$$\frac{\mathrm{D}\boldsymbol{u}}{\mathrm{D}t} = \frac{2}{\rho} \boldsymbol{\nabla} \cdot (\rho \nu \mathbf{S}) - \frac{1}{4} \boldsymbol{\nabla} \ln \rho + \frac{\boldsymbol{u}}{3} (\boldsymbol{\nabla} \cdot \boldsymbol{u} + \boldsymbol{u} \cdot \boldsymbol{\nabla} \ln \rho) - \frac{\boldsymbol{u}}{\rho} [\boldsymbol{u} \cdot (\boldsymbol{J} \times \boldsymbol{B}) + \eta \boldsymbol{J}^2] + \frac{3}{4\rho} \boldsymbol{J} \times \boldsymbol{B}, \tag{4}$$

$$\frac{\partial \ln \rho}{\partial t} = -\frac{4}{3} (\boldsymbol{\nabla} \cdot \boldsymbol{u} + \boldsymbol{u} \cdot \boldsymbol{\nabla} \ln \rho) + \frac{1}{\rho} [\boldsymbol{u} \cdot (\boldsymbol{J} \times \boldsymbol{B}) + \eta \boldsymbol{J}^2],$$

$$\frac{\partial^2}{\partial t^2} \tilde{h}_{+/\times}(\boldsymbol{k}, t) + k^2 \tilde{h}_{+/\times}(\boldsymbol{k}, t) = \frac{6}{t} \tilde{T}_{+/\times}(\boldsymbol{k}, t)$$

GWs sourced by stress $\mathsf{T}_{ij} = \frac{4}{3}\gamma_{\mathrm{Lor}}^2 \rho u_i u_j - B_i B_j + \ldots$

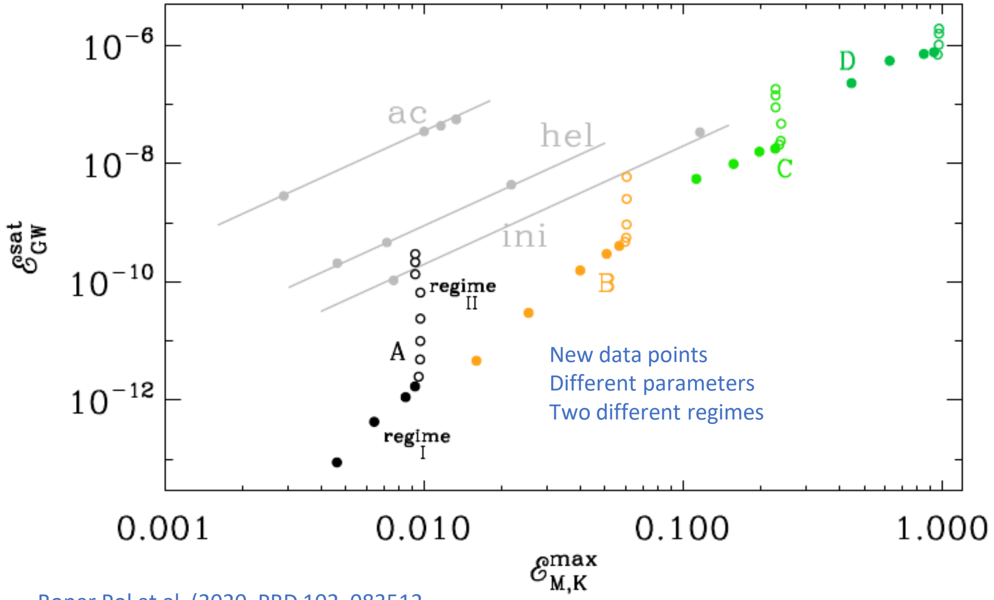

Roper Pol et al. (2020, PRD 102, 083512

Observability of relic GWs

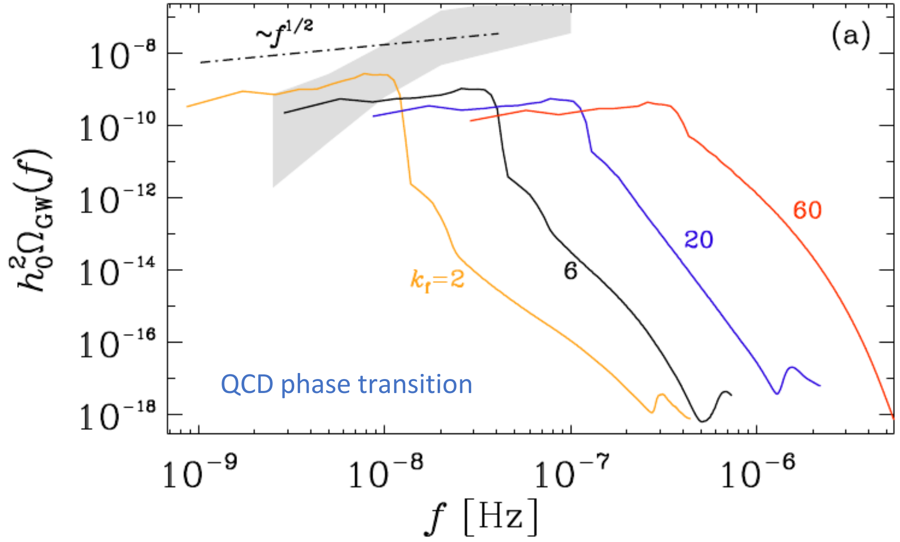

NANOGrav = North American nHz Obs for GWs
Neronov et al. (2021, PRD 103, 041302)
Brandenburg et al. (arXiv:2102.12428)

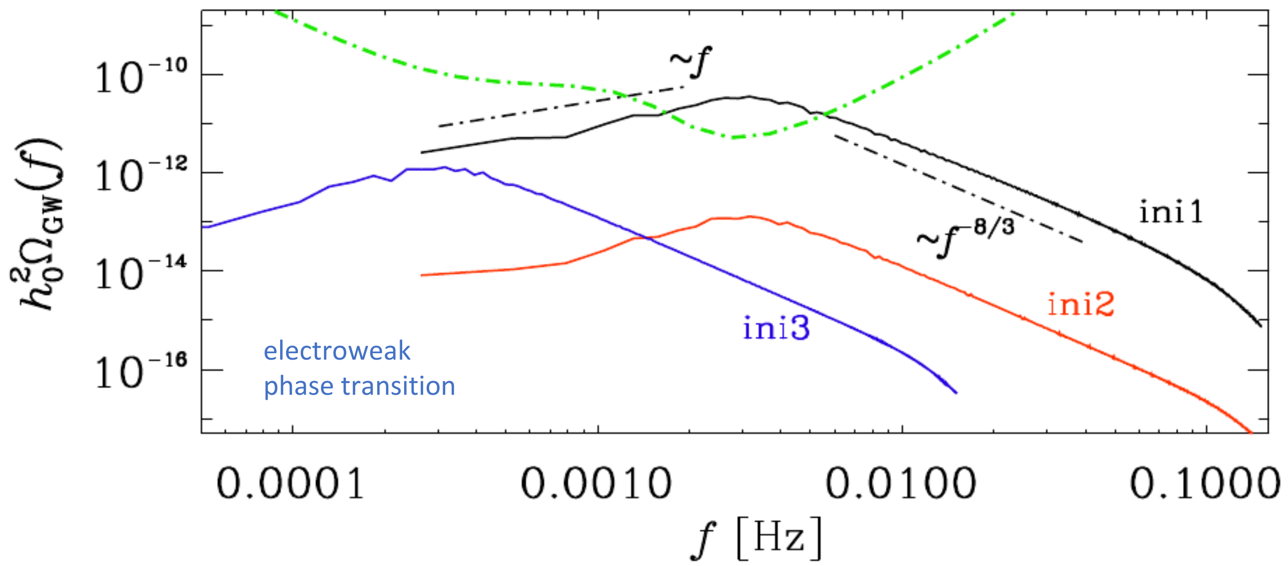

LISA = Laser Interferometer Space Antenna
Roper Pol et al. (2020, PRD 102, 083512)

Brandenburg et al. (2017, PRD 96, 123528)

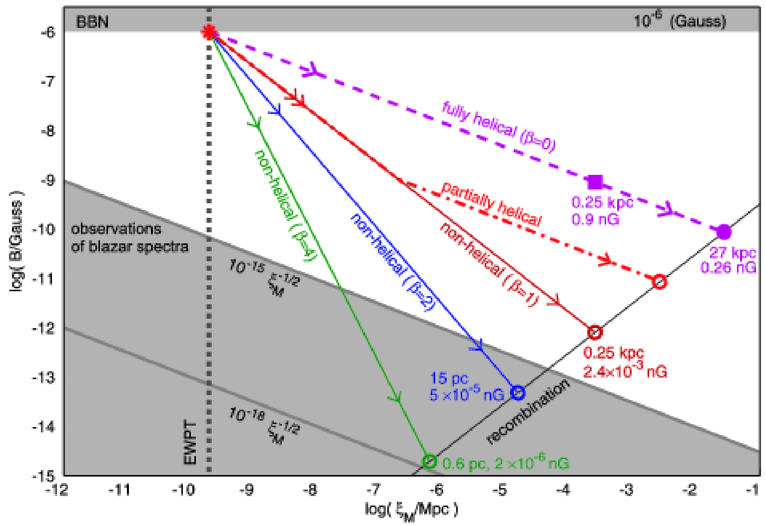

- GWs driven by magnetic stress, B ~ 1 μG
  - 1 μG would have decayed to 0.3 nG at 30 kpc
- Lower limits from Fermi LAT (Large Area Telesc)
  - 10^{-15} G at 1 Mpc (Neronov & Vovk 2010)
  - Already well above chiral B-field limit of 10^{-18} G
- B-fields driven at hoc (no magnetogenesis)

Spectral correspondence

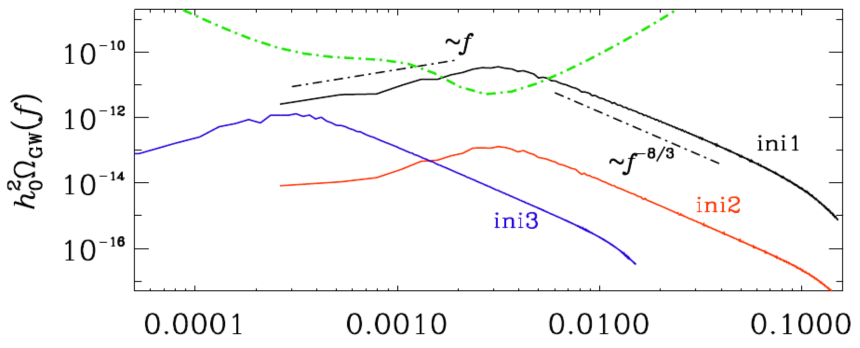

Turbulent intertial range

- B spectrum $E(k)$ = Sp(B) ~ $k^{-5/3}$
- Stress spectrum Sp(B_i B_j) ~ $k^{-5/3}$
  (Brandenburg & Boldyrev 2020)
- Therefore Sp($k^2 h_{ij}$) ~ $k^{-5/3}$
- So $E_{\rm GW}(k)$ ~ Sp(kh_{ij}) ~ k^{-2} Sp($k^2 h_{ij}$) ~ $k^{-11/3}$
- and $\Omega_{\rm GW}(k) = kE_{\rm GW}$(k) ~$k^{-8/3}$

Subintertial range

- B spectrum $E(k)$ = Sp(B) ~ k^4
- Stress spectrum Sp(B_i B_j) ~ k^2,
- not k^4 (Brandenburg & Boldyrev 2020)
- Therefore Sp($k^2 h_{ij}$) ~ k^2, not k^4
- So $E_{\rm GW}(k)$ ~ Sp(kh_{ij}) ~ k^0, not k^2
- and $\Omega_{\rm GW}(k) = kE_{\rm GW}$(k) ~$k^1$, not k^3

Simple example

$$\left(\partial_t^2 + 3H\partial_t - c^2\nabla^2\right) h_{ij}(\boldsymbol{x},t) = \frac{16\pi G}{c^2}\, T_{ij}^{\rm TT}(\boldsymbol{x},t)$$

$$T_{ij}(\boldsymbol{x},t) = \left(p/c^2+\rho\right)\gamma^2 u_i u_j - B_i B_j + (\boldsymbol{B}^2/2+p)\delta_{ij}$$

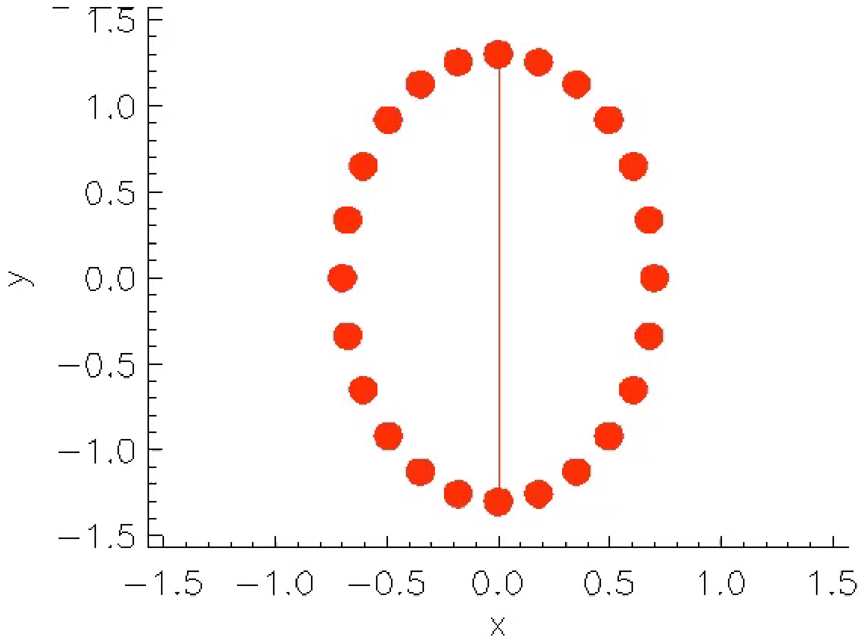

Example

$$\boldsymbol{B} = \begin{pmatrix} 0 \\ \sigma\sin kx \\ \cos kx \end{pmatrix} \longrightarrow \boldsymbol{\nabla}\times\boldsymbol{B} = \begin{pmatrix} \partial_x \\ 0 \\ 0 \end{pmatrix} \times \begin{pmatrix} 0 \\ \sin kx \\ \cos kx \end{pmatrix} = k \begin{pmatrix} 0 \\ \sin kx \\ \cos kx \end{pmatrix} = k\boldsymbol{B}$$

GW energy dependence on magnetic energy and wavenumber k0.

$$\bar{\Omega}_{\rm GW} = \frac{3H_*^2}{c^2k_0^2}\,\Omega_{\rm M}^2$$

Roper Pol et al. (2020, GAFD 114, 130)

Traceless-transverse

$$T_{ij}(x) = \mathcal{E}_{\rm M}\begin{pmatrix} 0 & 0 & 0 \\ 0 & -\cos 2kx & \sigma\sin 2kx \\ 0 & \sigma\sin 2kx & \cos 2kx \end{pmatrix}$$

Polarization in turbulent cases:
Kahniashvili et al. (2021, PRR 3, 013193)

Different efficiencies

$$\mathcal{E}_{\rm GW}^{\rm sat} \approx (q\mathcal{E}_{\rm M}^{\rm max}/k_{\rm peak})^2$$

- Efficiency q between 1 and 30
- Acoustic turbulence more efficient
- Is TT projection different for acoustic turbulence?

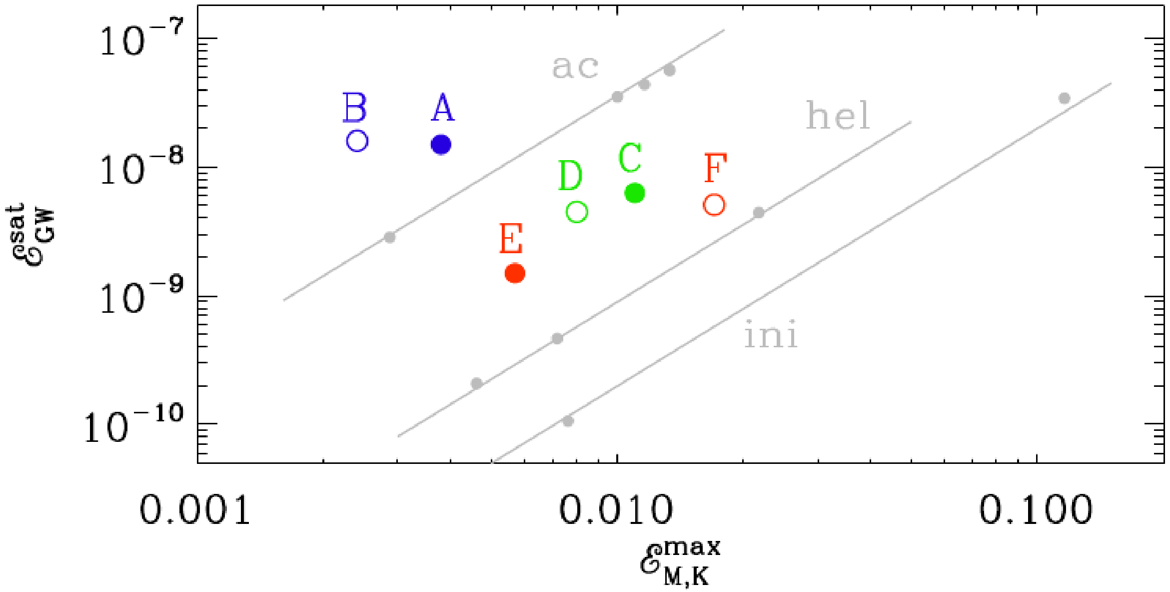

Run	i	k_*	$\mathcal{E}_i^{\rm max}$	σ	wave	$\mathcal{E}_{\rm GW}^{\rm sat}$	$\nu\ (=\eta)$	f_0	q
A	Ka	600	3.8×10^{-3}	0	expan	1.5×10^{-8}	10^{-6}	1	19
B	Ka	600	2.4×10^{-3}	0	plane	1.6×10^{-8}	2×10^{-7}	2×10^{-3}	32
C	Kv	600	8.0×10^{-3}	0	plane	4.5×10^{-9}	2×10^{-7}	4×10^{-1}	4.3
D	Kv	600	1.1×10^{-2}	1	plane	6.3×10^{-9}	2×10^{-7}	4×10^{-1}	5.0
E	Mv	600	5.7×10^{-3}	0	plane	1.5×10^{-9}	2×10^{-7}	6×10^{-4}	4.1
F	Mv	600	1.7×10^{-2}	1	plane	5.1×10^{-9}	2×10^{-7}	6×10^{-4}	2.5
G	Ka	2	4.2×10^{-2}	0	plane	8.3×10^{-4}	2×10^{-2}	7×10^{-1}	1.4
H	Kv	2	4.7×10^{-2}	0	plane	1.1×10^{-3}	1×10^{-2}	4×10^{-1}	1.4

- How is q related to temporal properties?
- Need to study GWs from selfconsistent magnetogenesis
- Chiral magnetic effect one example (studied previously)
- Even if looking under a lampost

Scalar-Vector-Tensor decomposition

$$\lambda_{ij} = L\delta_{ij} + \nabla_{\langle i}\nabla_{j\rangle}\lambda + \nabla_{(i}\bar{\lambda}_{j)} + \bar{\lambda}_{ij};$$

- Trace L
- traceless Hessian of scalar
- Symmetrized gradient tensor
- Pure tensor mode

  - Acoustic turbulence: small tensor mode
  - Except small k ←
  - How import is contribution from frequencies ω ~ *ck* ?

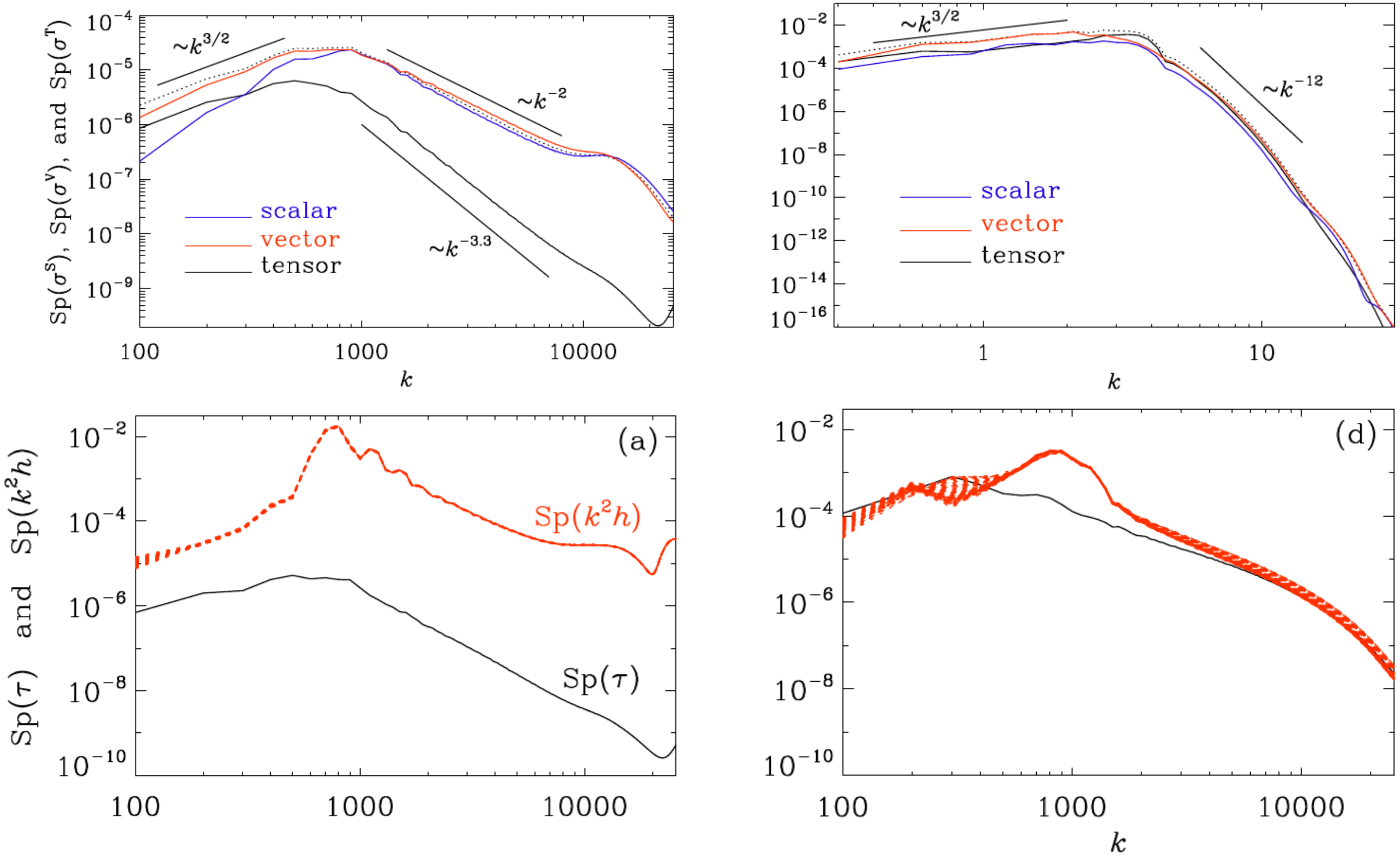

Time dependence from chiral magnetic effect (CME)

- Exponential growth at one k
- Subsequent inverse cascade
- Always fully helical

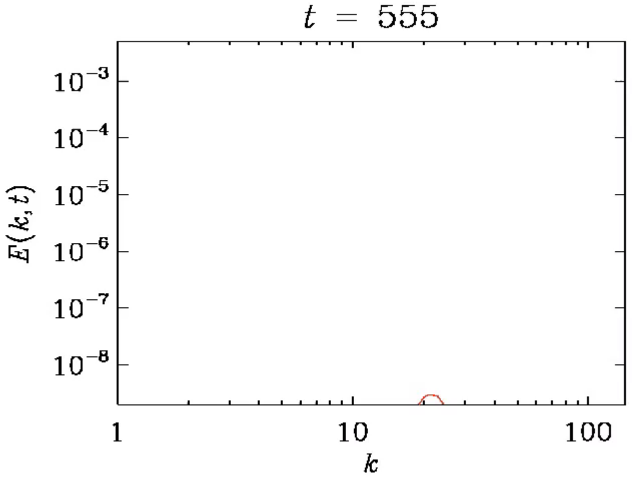

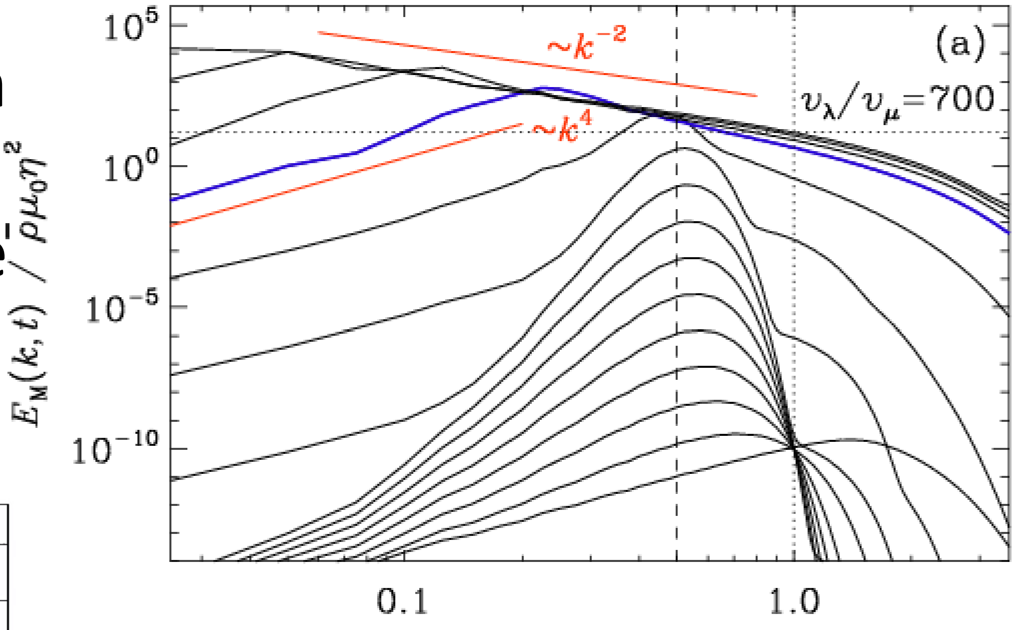

Growth at one wavenumber
Then: saturation caused by initial chemical potential

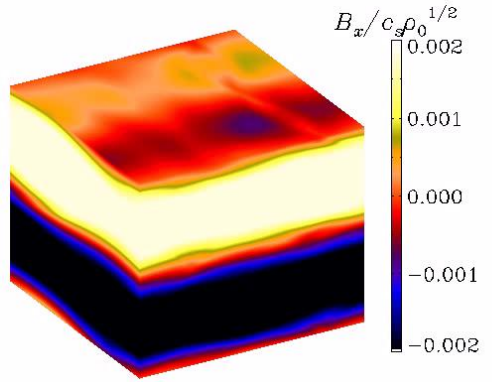

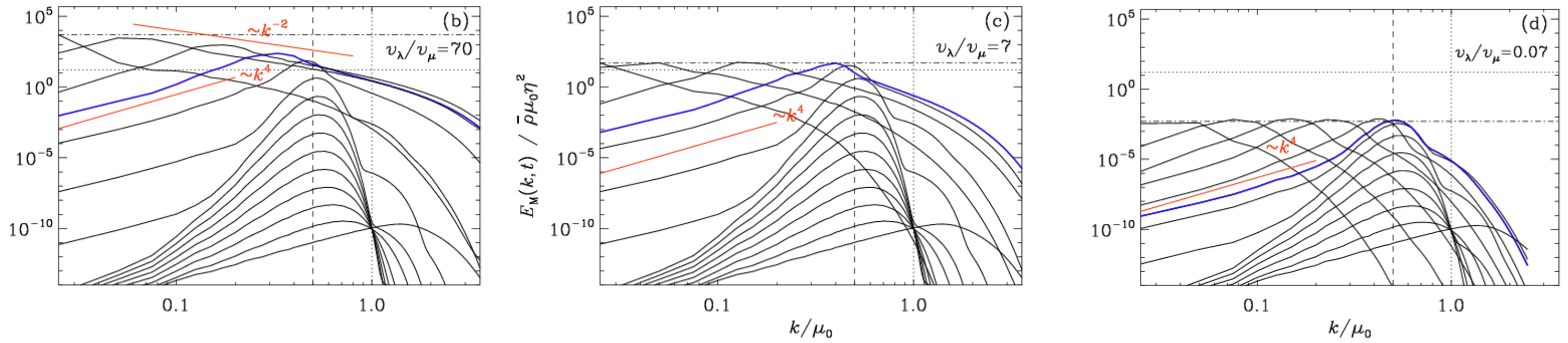

Brandenburg et al. (2017, ApJL 845, L21)

CME introduces pseudoscalar

- Mathematically identical to α effect in mean-field dynamos
- Comes from chiral chemical potential μ (or μ_5)
- Number differences of left- & right-handed fermions

$$\mu_5 = 24\,\alpha_{\rm em}\,(n_{\rm L} - n_{\rm R})\,(\hbar c/k_{\rm B}T)^2,$$

- In the presence of a magnetic field, particles of opposite charge have momenta
- → electric current
- Self-excited dynamo
- But depletes μ

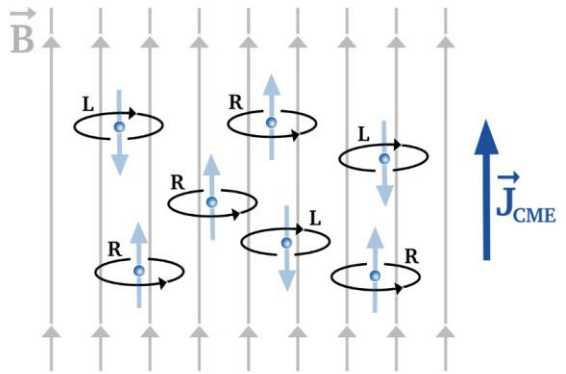

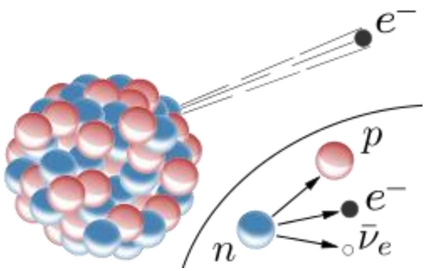

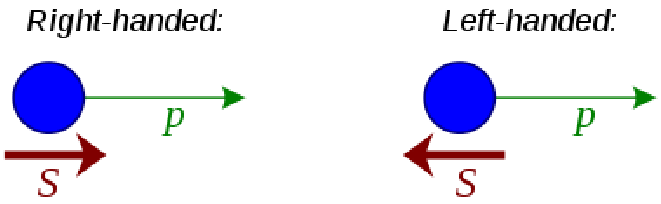

$$\frac{\partial \boldsymbol{A}}{\partial t} = \eta(\mu \boldsymbol{B} - \boldsymbol{\nabla} \times \boldsymbol{B}) + \boldsymbol{U} \times \boldsymbol{B}$$

$$\sigma = |\mu k| - \eta k^2$$

B=curlA

Many details are known by now

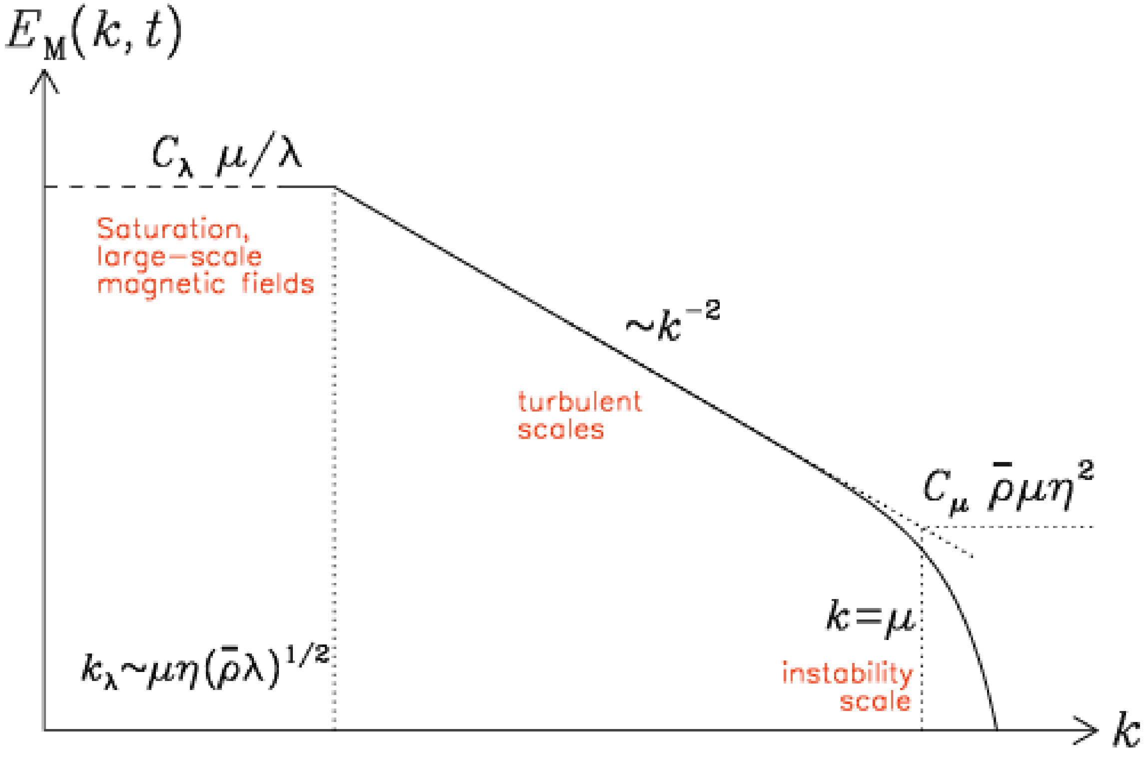

- Instability just η dependant
- Saturation governed by λ

- Regime I is when turbulent subrange is long
- In regime II, just inverse cascading

$$\frac{\partial \boldsymbol{B}}{\partial t} = \boldsymbol{\nabla} \times [\boldsymbol{u} \times \boldsymbol{B} + \eta(\mu_5 \boldsymbol{B} - \boldsymbol{J})], \quad \boldsymbol{J} = \boldsymbol{\nabla} \times \boldsymbol{B},$$

$$\frac{\mathrm{D}\mu_5}{\mathrm{D}t} = -\lambda\,\eta\,(\mu_5 \boldsymbol{B} - \boldsymbol{J}) \cdot \boldsymbol{B} + D_5 \nabla^2 \mu_5 - \Gamma_{\mathrm{f}} \mu_5,$$

$$v_\lambda = \mu_{50}/\lambda^{1/2}, \qquad v_\mu = \mu_{50}\eta. \tag{6}$$

We recall that we have used here dimensionless quantities. We can identify two regimes of interest:

$$\eta k_1 < v_\mu < v_\lambda \quad \text{(regime I)}, \tag{7}$$

$$\eta k_1 < v_\lambda < v_\mu \quad \text{(regime II)}, \tag{8}$$

Strength of chiral magnetic effect

- Dimensional arguments give

$$\langle \boldsymbol{B}^2 \rangle \, \xi_{\mathrm{M}} = \epsilon \, (k_{\mathrm{B}} T_0)^3 (\hbar c)^{-2},$$

- Inserting T=3K gives 10^{-18} G on 1 Mpc
- But starting length scale very small
- → 12 cm
- Compared with horizon scale at that time (electroweak) of ~1 AU
- Other dimensional argument:

$$\langle \boldsymbol{B}^2 \rangle \xi_{\mathrm{M}} \lesssim \epsilon_3 (a_\star / a_0)^3 G^{-3/2} \hbar^{-1/2} c^{11/2},$$

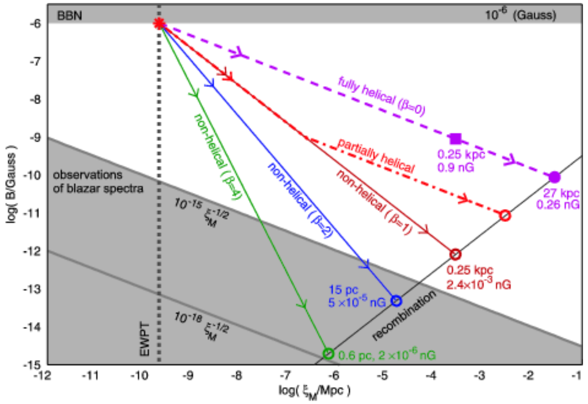

Another severe problem are the very small length scales associated with the CME. An upper bound for the wavenumber associated with the chiral asymmetry in comoving units is $k_* \equiv k_{\mathrm{B}}T/\hbar c = 12\,\mathrm{cm}^{-1}$, where k_{B} is the Boltzmann constant, $\hbar$ is the reduced Planck constant, c is the speed of light, and $T = 2.7\,\mathrm{K}$ is the present day temperature. Assuming a field strength of $1\,\mu\mathrm{G}$, the

- Would like something like:

$$\langle \boldsymbol{B}^2 \rangle \xi_{\mathrm{M}} \lesssim \epsilon_2^{2/3} \epsilon_3^{1/3} (a_\star / a_0) (k_{\mathrm{B}} T_0)^2 G^{-1/2} \hbar^{-3/2} c^{1/2},$$

$$v_\lambda = \mu_{50}/\lambda^{1/2}, \qquad v_\mu = \mu_{50}\eta. \tag{6}$$

We recall that we have used here dimensionless quantities. We can identify two regimes of interest:

$$\eta k_1 < v_\mu < v_\lambda \quad \text{(regime I)}, \tag{7}$$

$$\eta k_1 < v_\lambda < v_\mu \quad \text{(regime II)}, \tag{8}$$

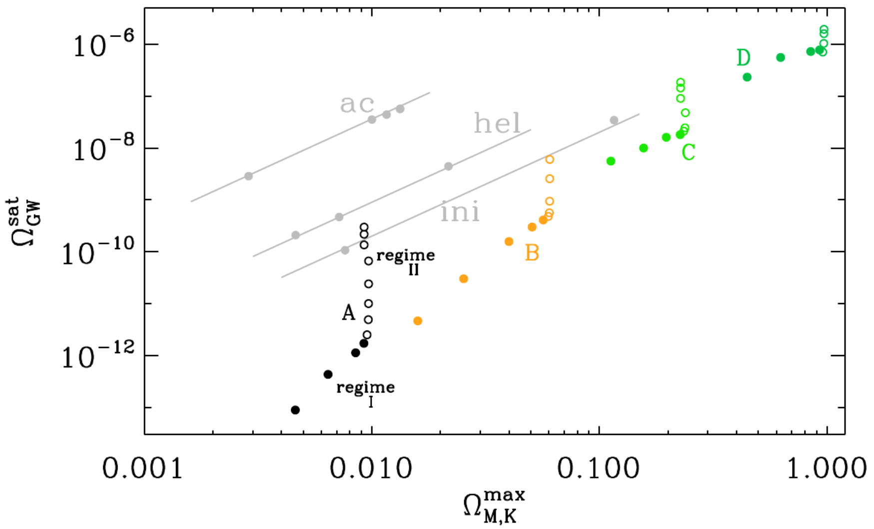

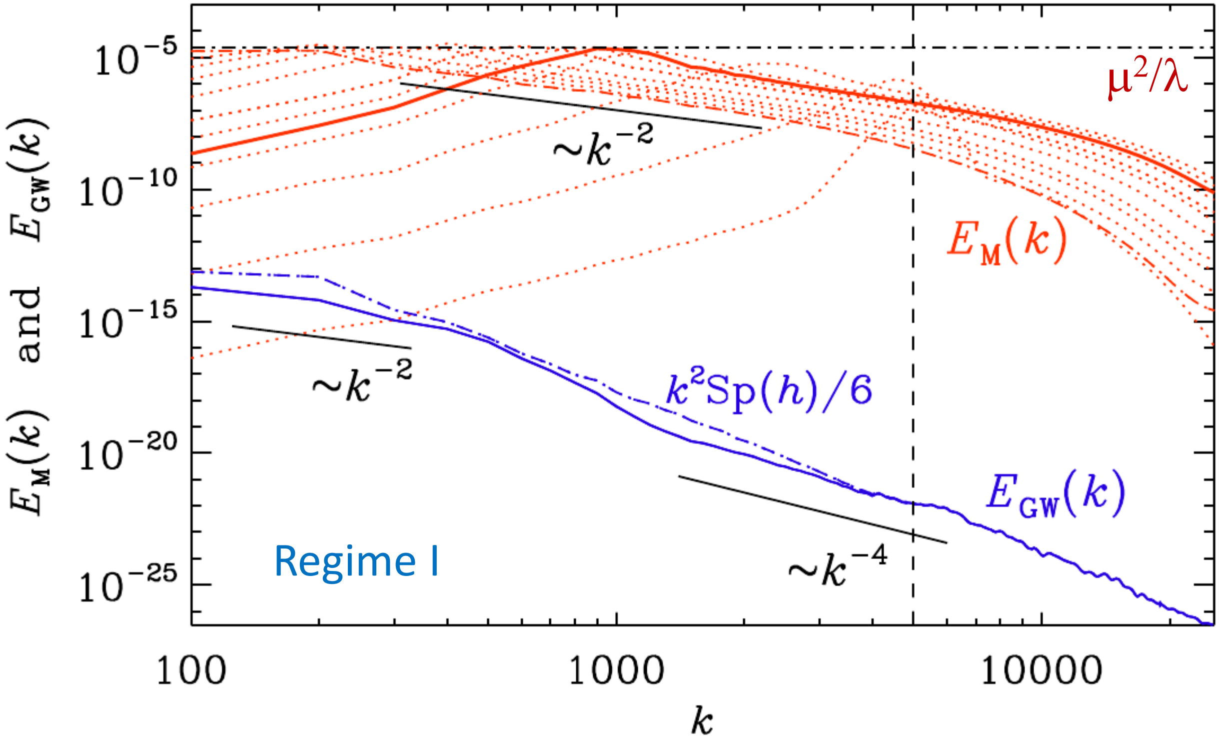

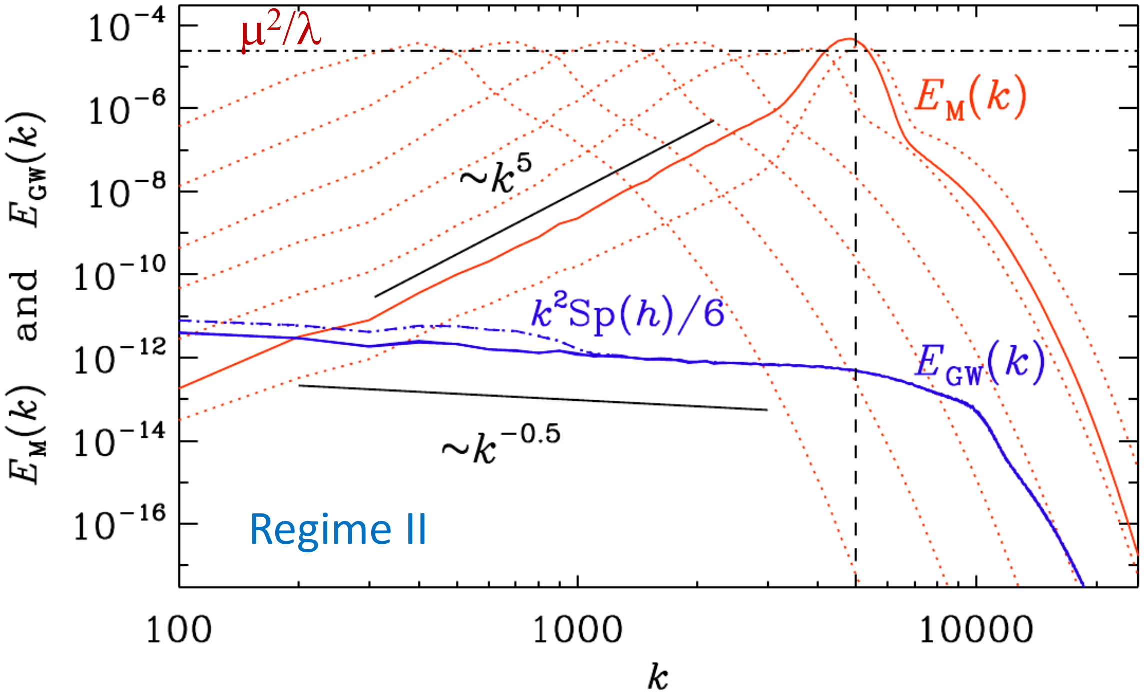

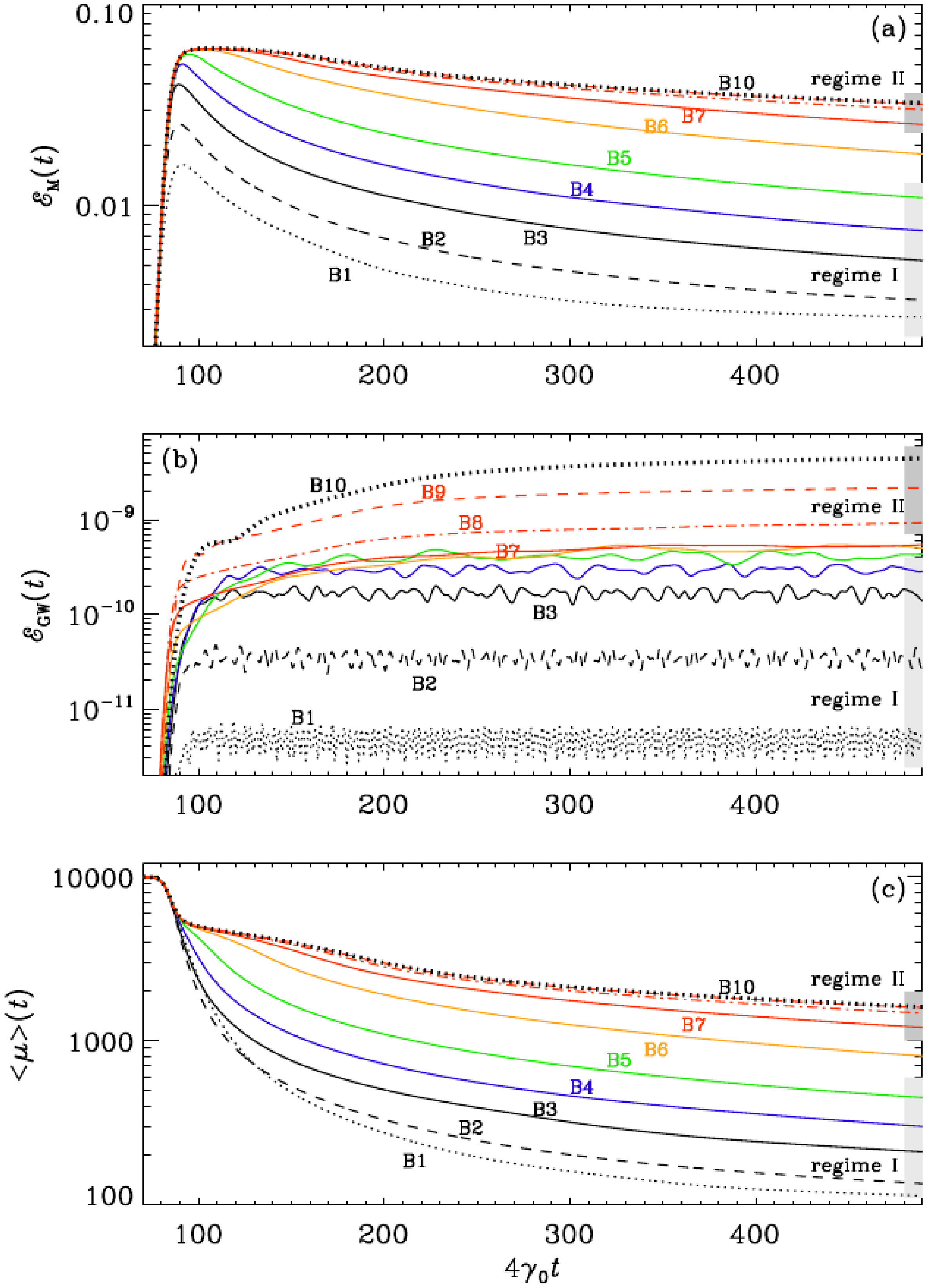

Time trace of magn & GW energies

- For Runs B1 → B10, η increase 10^{-6} → 10^{-3}
  - Therefore, growth rate $\gamma=\eta\mu^2/4$ increases
- Peak magnetic energy reached when γt=20
  - Depends on initial & final $\mathcal{E}_M=\mu^2/\lambda$
- $\mathcal{E}_{GW}$ saturation depends on regime
  - Regime I (B1-B5), $\mathcal{E}_{GW}$ saturates at peak
  - Regime II (B6-B10), $\mathcal{E}_{GW}$ saturation prolonged
- μ depletion also different
  - Faster in Regime I, when linear growth fast
- What prolonged saturation behavior?

  → Change of slope at late times

Regime I

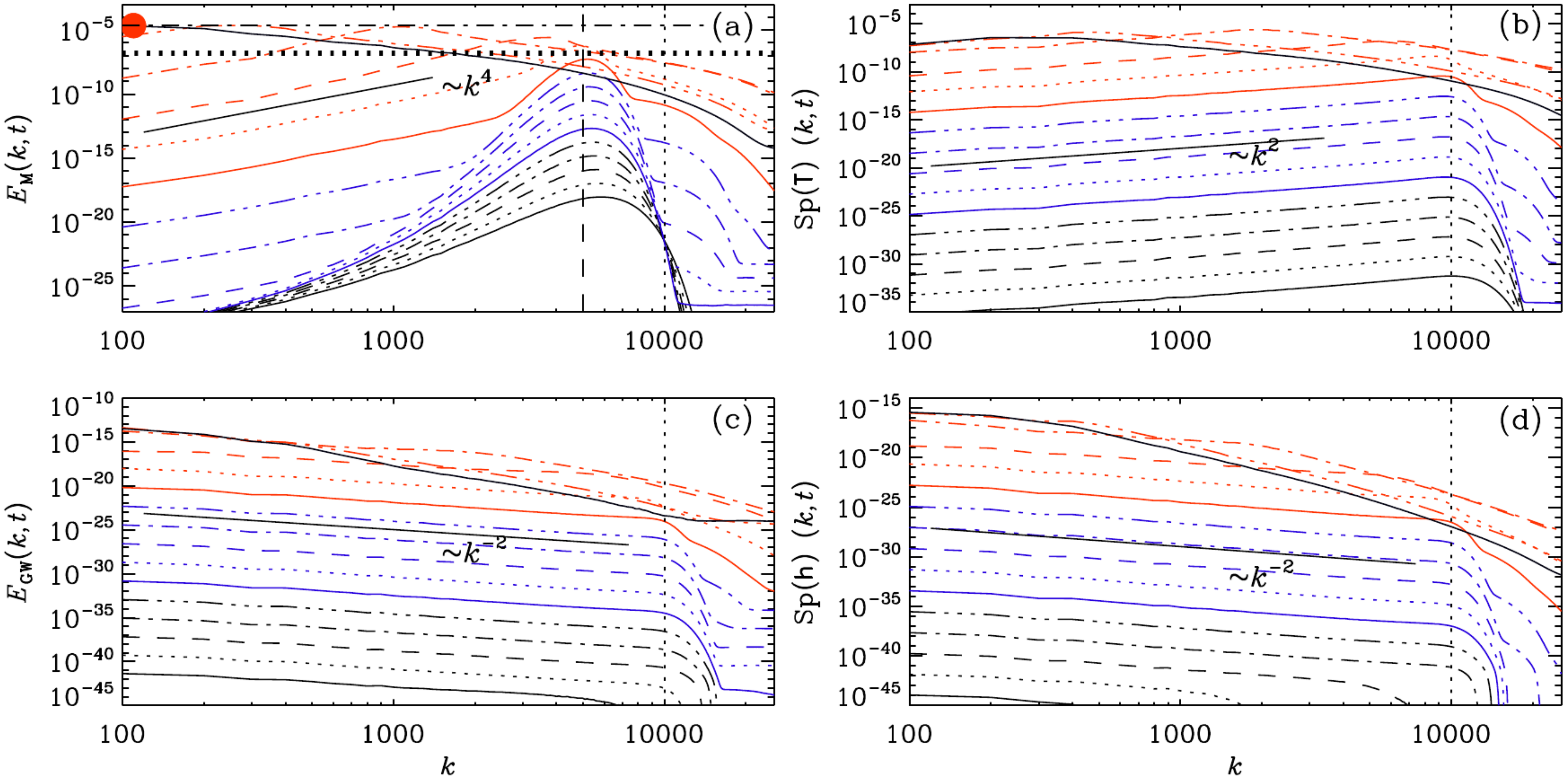

(a)
(b)
(c)
(d)
$\sim k^4$
$\sim k^2$
$\sim k^{-2}$
$\sim k^{-2}$
$E_M(k,t)$
$\mathrm{Sp(T)}\ (k,t)$
$E_{GW}(k,t)$
$\mathrm{Sp(h)}\ (k,t)$
k
k
100
1000
10000

Regime II

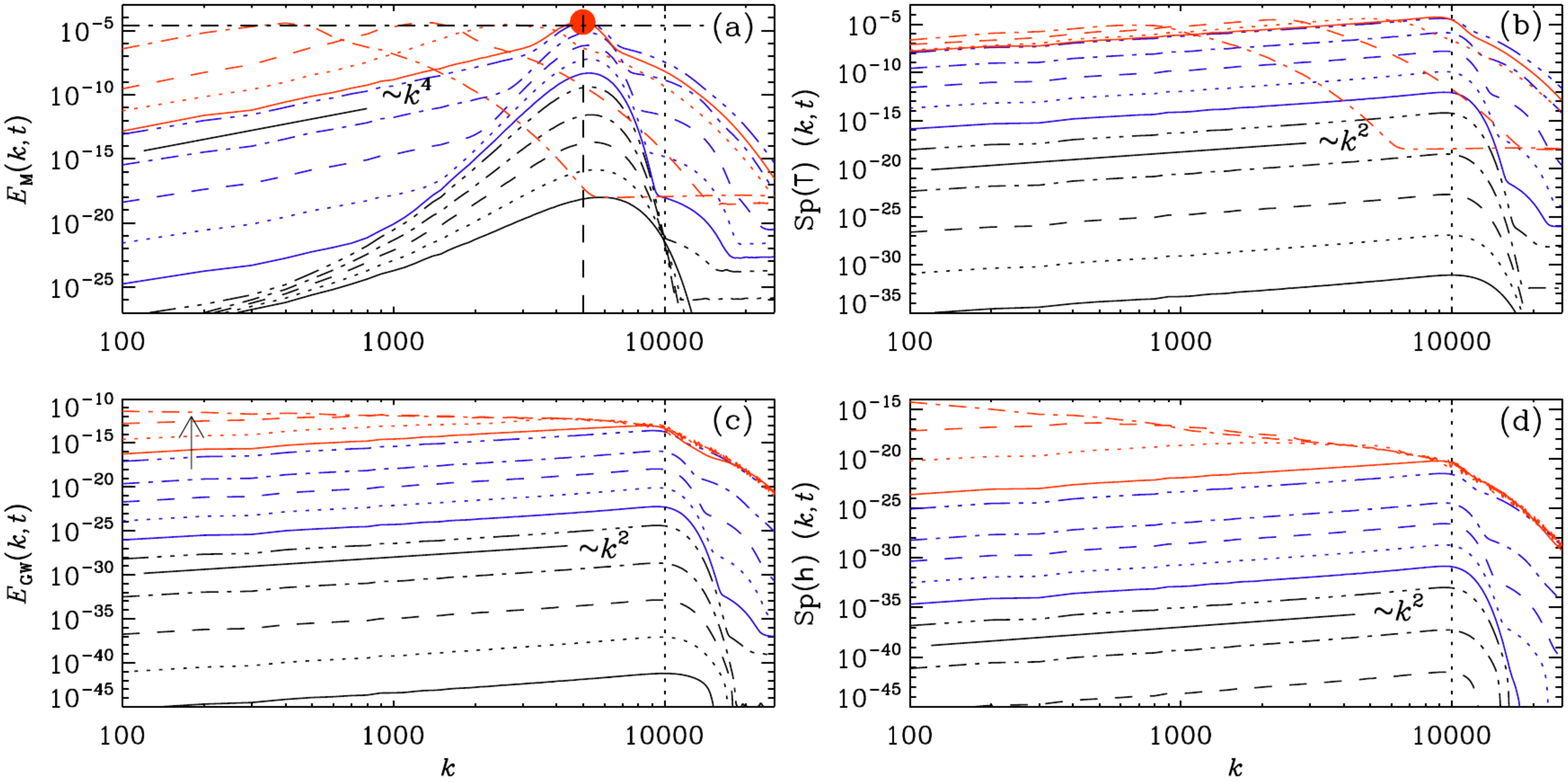

(a)
(b)
(c)
(d)
$E_M(k,t)$
$Sp(T)\ (k,t)$
$E_{GW}(k,t)$
$Sp(h)\ (k,t)$
$\sim k^4$
$\sim k^2$
$\sim k^2$
$\sim k^2$
k
k
100
1000
10000

Early kinematic growth phase

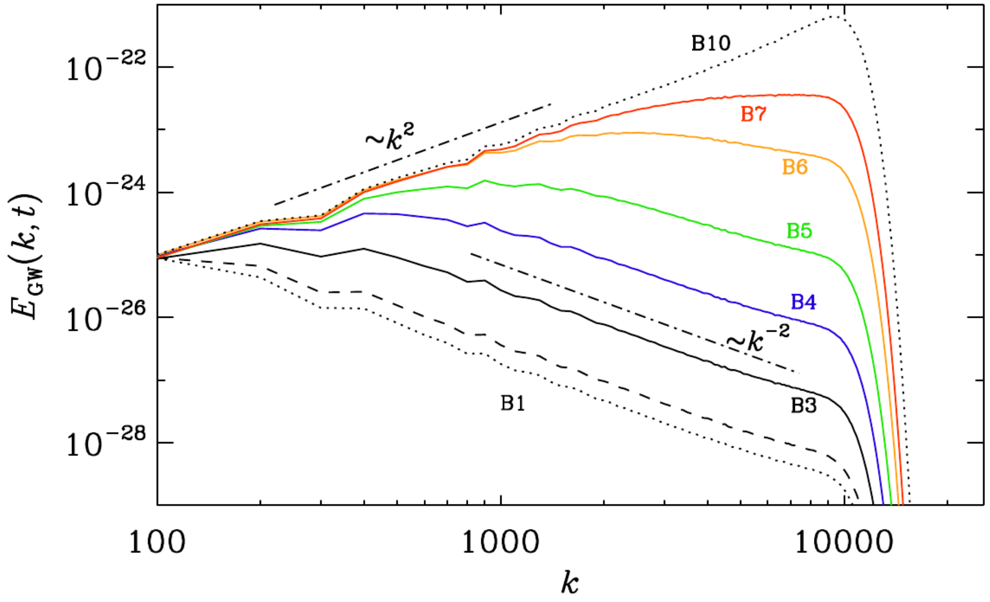

$$\tilde{T}(\boldsymbol{k},t) = \theta(t-1)\,\tilde{T}_0(k)\,e^{2\gamma_0(t-1)}, \tag{16}$$

where $\theta(t)$ is the Heaviside step function, and $\tilde{T}_0(k)$ is assumed to depend just on $k = |\boldsymbol{k}|$.

Using $\tilde{h}(k,1) = \dot{\tilde{h}}(k,1) = 0$ as initial conditions, we can solve Equation (5) during the early growth phase in closed form as

$$\tilde{h}(k,t) = \frac{6\tilde{T}_0(k)}{4\gamma_0^2 + k^2}\left[e^{2\gamma_0\tau} - \cos k\tau - \frac{2\gamma_0}{k}\sin k\tau\right]_{\tau=t-1}, \tag{17}$$

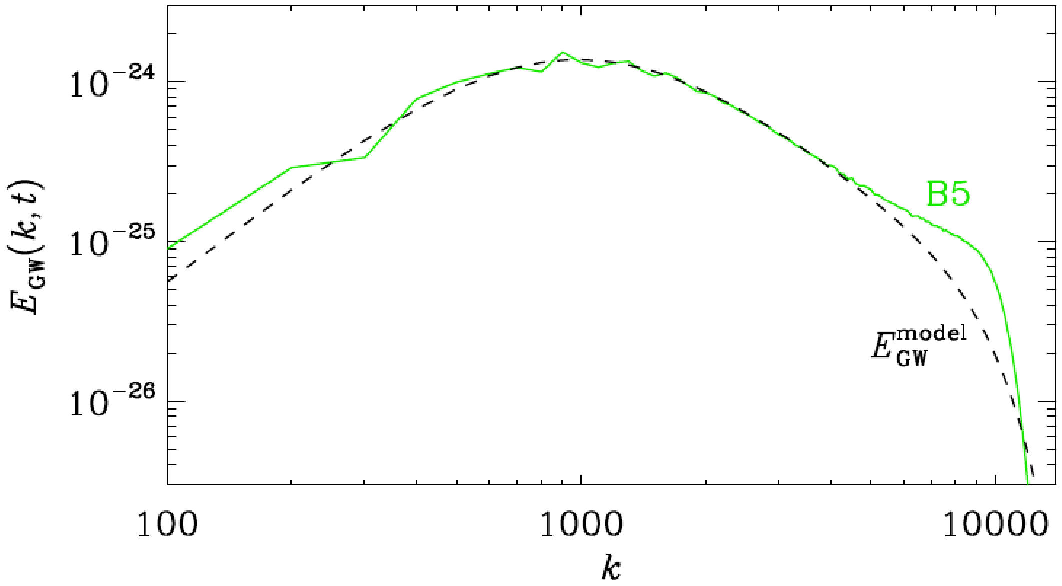

Saturated phase: scaling

$$v_\lambda = \mu_{50}/\lambda^{1/2}, \qquad v_\mu = \mu_{50}\eta. \tag{6}$$

We recall that we have used here dimensionless quantities. We can identify two regimes of interest:

$$\eta k_1 < v_\mu < v_\lambda \quad \text{(regime I)}, \tag{7}$$

$$\eta k_1 < v_\lambda < v_\mu \quad \text{(regime II)}, \tag{8}$$

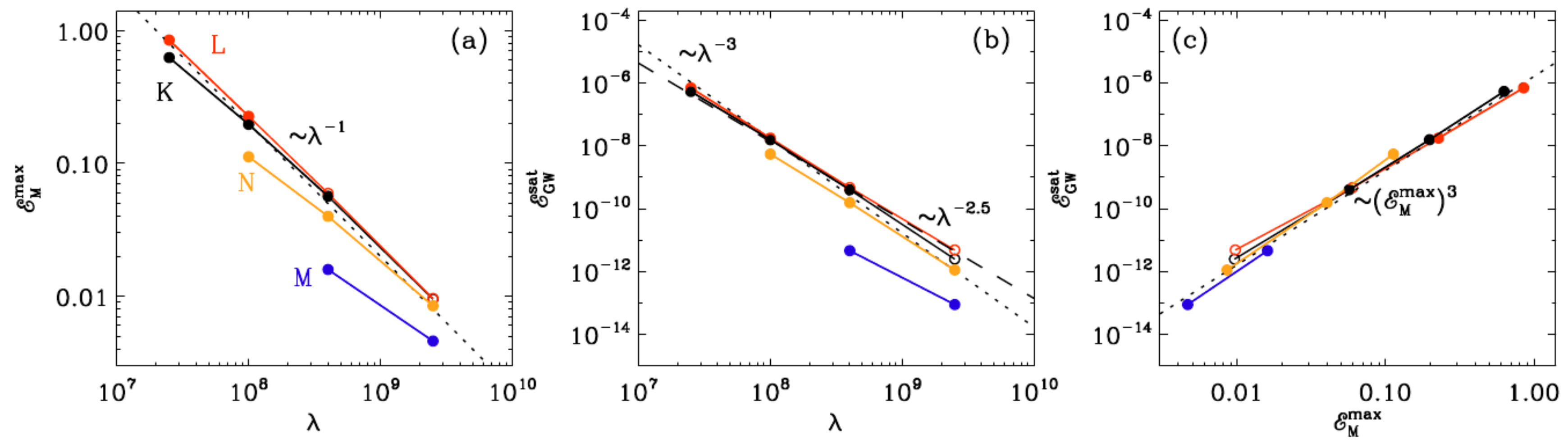

FIG. 11.— Dependence of $\mathcal{E}_{\rm M}^{\rm max}$ and $\mathcal{E}_{\rm GW}^{\rm sat}$ on λ, and their mutual parametric dependence for runs of series K–N. Filled (open) symbols denote runs in regime I (II). The dotted line in panel (c) is for $q = 7\,\mathcal{E}_{\rm M}^{\rm max}$.

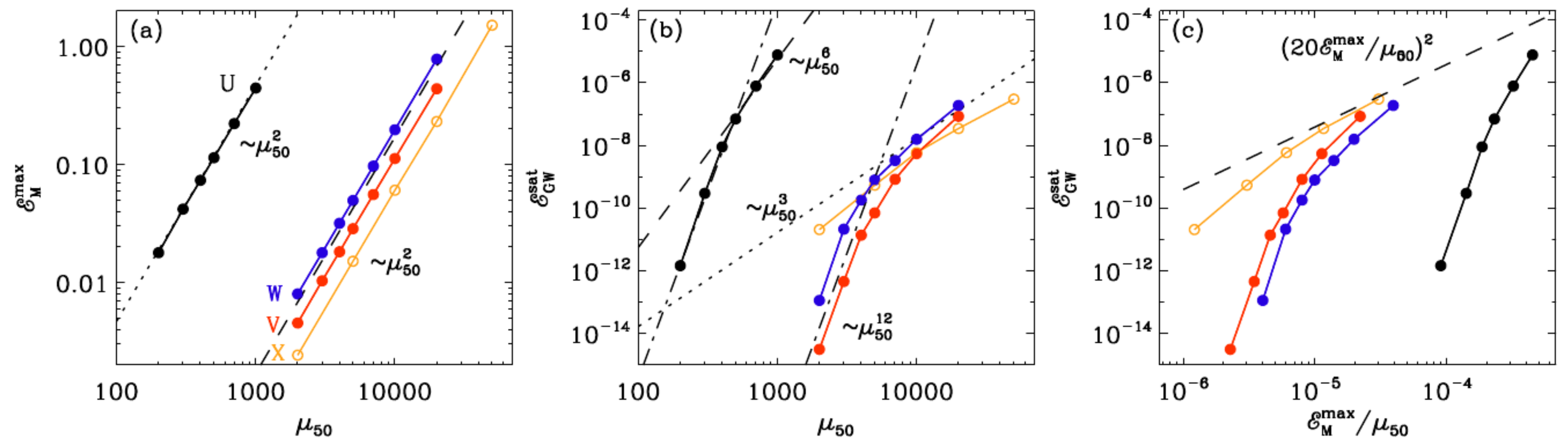

FIG. 12.— Dependence of $\mathcal{E}_{\rm M}^{\rm max}$ and $\mathcal{E}_{\rm GW}^{\rm sat}$ on μ_{50}, and their mutual parametric dependence for runs of series U–X. Filled (open) symbols denote runs in regime I (II). The dashed line in panel (c) is for $q = 20$.

Saturated phase phase

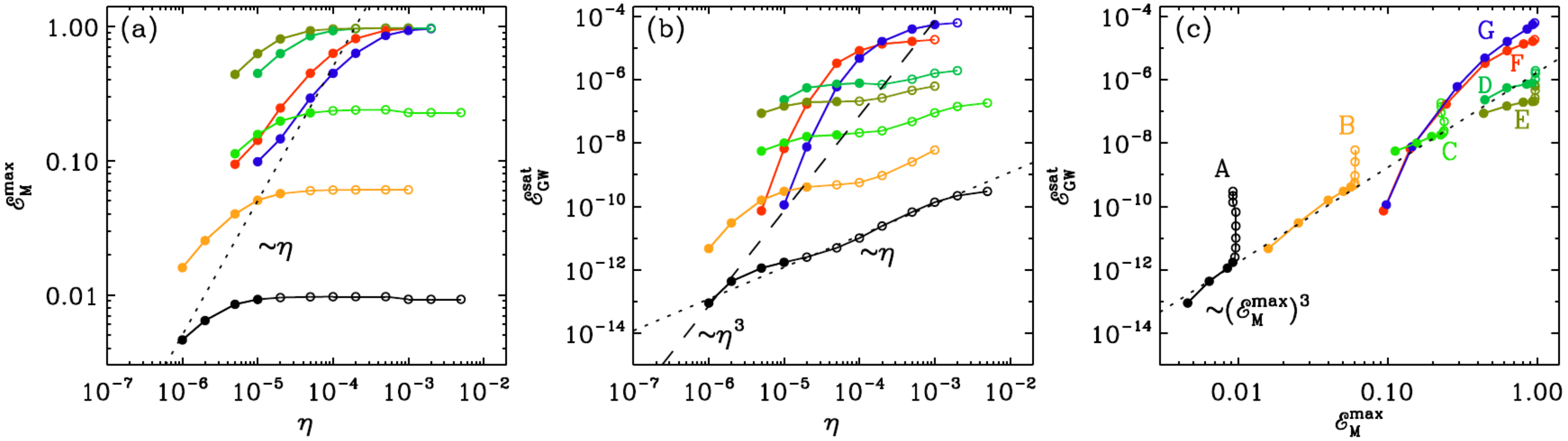

Saturated phase: scaling

$$v_\lambda = \mu_{50}/\lambda^{1/2}, \qquad v_\mu = \mu_{50}\eta. \tag{6}$$

We recall that we have used here dimensionless quantities. We can identify two regimes of interest:

$$\eta k_1 < v_\mu < v_\lambda \quad \text{(regime I)}, \tag{7}$$

$$\eta k_1 < v_\lambda < v_\mu \quad \text{(regime II)}, \tag{8}$$

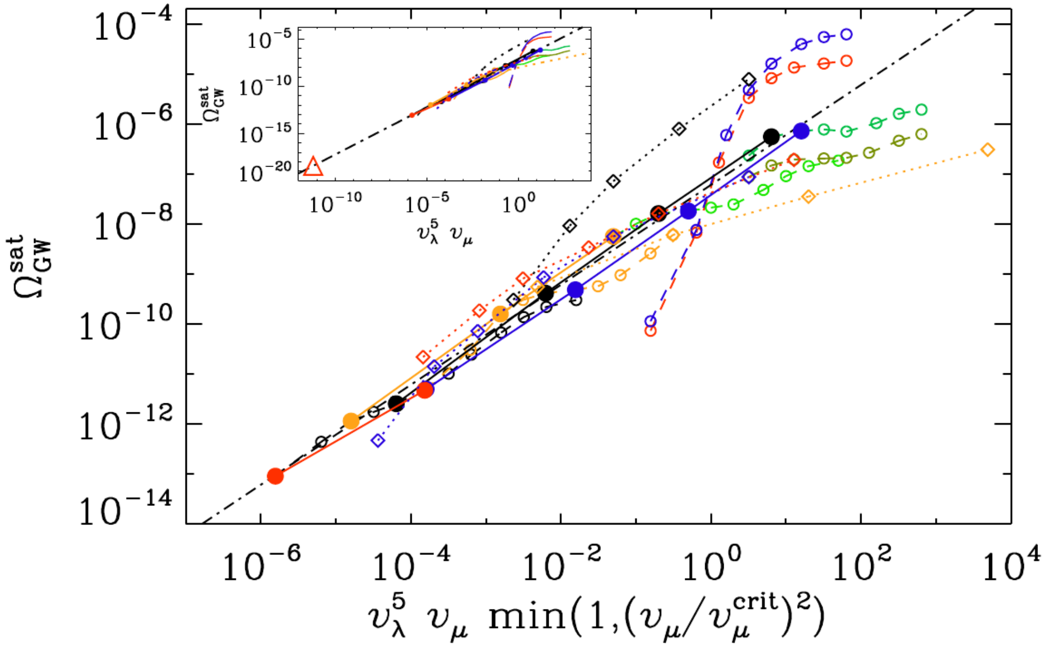

Code & data public

- JOSS = Journal of Open Source Software

The Journal of Open Source Software

The Pencil Code, a modular MPI code for partial differential equations and particles: multipurpose and multiuser-maintained

The Pencil Code Collaboration[1], Axel Brandenburg[1, 2, 3], Anders Johansen[4], Philippe A. Bourdin[5, 6], Wolfgang Dobler[7], Wladimir Lyra[8], Matthias Rheinhardt[9], Sven Bingert[10], Nils Erland L. Haugen[11, 12, 1], Antony Mee[13], Frederick Gent[9, 14], Natalia Babkovskaia[15], Chao-Chin Yang[16], Tobias Heinemann[17], Boris Dintrans[18], Dhrubaditya Mitra[1], Simon Candelaresi[19], Jörn Warnecke[20], Petri J. Käpylä[21], Andreas Schreiber[15], Piyali Chatterjee[22], Maarit J. Käpylä[9, 20], Xiang-Yu Li[1], Jonas Krüger[11, 12], Jørgen R. Aarnes[12], Graeme R. Sarson[14], Jeffrey S. Oishi[23], Jennifer Schober[24], Raphaël Plasson[25], Christer Sandin[1], Ewa Karchniwy[12, 26], Luiz Felippe S. Rodrigues[14, 27], Alexander Hubbard[28], Gustavo Guerrero[29], Andrew Snodin[14], Illa R. Losada[1], Johannes Pekkilä[9], and Chengeng Qian[30]

1 Nordita, KTH Royal Institute of Technology and Stockholm University, Sweden **2** Department of Astronomy, Stockholm University, Sweden **3** McWilliams Center for Cosmology & Department of Physics, Carnegie Mellon University, PA, USA **4** GLOBE Institute, University of Copenhagen, Denmark **5** Space Research Institute, Graz, Austria **6** Institute of Physics, University of Graz, Graz, Austria **7** Bruker, Potsdam, Germany **8** New Mexico State University, Department of Astronomy, Las Cruces, NM, USA **9** Astroinformatics, Department of Computer Science, Aalto University, Finland **10** Gesellschaft für wissenschaftliche Datenverarbeitung mbH Göttingen, Germany **11** SINTEF Energy Research, Trondheim, Norway **12** Norwegian University of Science and Technology, Norway **13** Bank of America Merrill Lynch, London, UK **14** School of Mathematics, Statistics and Physics, Newcastle University, UK **15** No current affiliation **16** University of Nevada, Las Vegas, USA **17** Niels Bohr International Academy, Denmark **18** CINES, Montpellier, France **19** School of Mathematics and Statistics, University of Glasgow, UK **20** Max Planck Institute for Solar System Research, Germany **21** Institute for Astrophysics, University of Göttinge, Germany **22** Indian Institute of Astrophysics, Bengaluru, India **23** Department of Physics & Astronomy, Bates College, ME, USA **24** Laboratoire d'Astrophysique, EPFL, Sauverny, Switzerland **25** Avignon Université, France **26** Institute of Thermal Technology, Silesian University of Technology, Poland **27** Radboud University, Netherlands **28** Department of Astrophysics, American Museum of Natural History, NY, USA **29** Physics Department, Universidade Federal de Minas Gerais, Belo Horizonte, Brazil **30** State Key Laboratory of Explosion Science and Technology, Beijing Institute of Technology, China

DOI: 10.21105/joss.02807

Software

- Review
- Repository
- Archive

Editor: Arfon Smith

Reviewers:

- @zingale
- @rtfisher

Submitted: 17 September 2020
Published: 21 February 2021

Summary

The Pencil Code is a highly modular physics-oriented simulation code that can be adapted to a wide range of applications. It is primarily designed to solve partial differential equations (PDEs) of compressible hydrodynamics and has lots of add-ons ranging from astrophysical magnetohydrodynamics (MHD) (A. Brandenburg & Dobler, 2010) to meteorological cloud microphysics (Li et al., 2017) and engineering applications in combustion (Babkovskaia et al., 2011). Nevertheless, the framework is general and can also be applied to situations not related to hydrodynamics or even PDEs, for example when just the message passing interface or input/output strategies of the code are to be used. The code can also evolve Lagrangian (inertial and noninertial) particles, their coagulation and condensation, as well as their interaction with the fluid. A related module has also been adapted to perform ray tracing

Conclusions

- Remarkably 2 different slopes for GW spectra
- Energy small, but may be different if active at early times

Early universe: use conservation law

Conseration equation $\tfrac{1}{2}\lambda \langle \boldsymbol{A}\cdot\boldsymbol{B}\rangle + \langle\mu\rangle = \mathrm{const} \equiv \mu_0 \quad (\text{for } \Gamma_\mathrm{f} \ll \eta\mu_0^2)$

$$(n_\mathrm{L} - n_\mathrm{R}) + \frac{4\alpha_\mathrm{em}}{\hbar c}\langle \boldsymbol{A}\cdot\boldsymbol{B}\rangle = \mathrm{const.}$$

Maximally helical: $\langle \boldsymbol{B}^2\rangle\, \xi_\mathrm{M} \lesssim \mu_0/\lambda.$

$$\langle \boldsymbol{B}^2\rangle\, \xi_\mathrm{M} = \epsilon\,(k_\mathrm{B}T_0)^3(\hbar c)^{-2},$$

Inserting actual numbers

Magnetic helicity

$$\langle \boldsymbol{B}^2 \rangle \, \xi_{\mathrm{M}} = \frac{\hbar c}{4\alpha_{\mathrm{em}}} \frac{g_0}{g_*} n_{\gamma 0} N_{\mathrm{f}} = 5 \times 10^{-38} \frac{N_{\mathrm{f}}}{10} g_{100}^{-1} \, \mathrm{G}^2 \, \mathrm{Mpc}. \quad (17)$$

Here, $g_0 = 3.36$ and $n_{\gamma 0} = 2\zeta(3)/\pi^2 (k_B T_0/\hbar c)^3 = 411 \ \mathrm{cm}^{-3}$

Inverse length scale

$$|\mu| \ll 4\alpha_{\mathrm{em}} \frac{k_{\mathrm{B}} T}{\hbar c} \approx 1.5 \times 10^{14} \, T_{100} \ \mathrm{cm}^{-1}$$

Inserting actual numbers (cont'd)

Magnetic diffusivity

(1.11) of Arnold et al. (2000):

$$\eta = 7.3 \times 10^{-4} \frac{\hbar c^2}{k_{\rm B} T} \approx 4 \times 10^{-9} T_{100}^{-1} \,{\rm cm}^2\,{\rm s}^{-1}. \qquad (19)$$

Thus, $v_\mu = 6 \times 10^5\,{\rm cm\,s}^{-1}$, so the number of e-folds is $\mathcal{N} \equiv v_\mu \mu / H \approx 5 \times 10^9\, g_{100}^{-1/2} T_{100}^{-1} \gg 1$, where $H^{-1} \approx 5 \times 10^{-11}\, g_{100}^{-1/2} T_{100}^{-2}$ s is the Hubble time.

Inserting actual numbers (cont'd)

Extent of cascade

$$\lambda = 3\hbar c \left(\frac{8\alpha_{\rm em}}{k_{\rm B}T} \right)^2 \approx 1.3 \times 10^{-17}\, T_{100}^{-2} \ \ \mathrm{cm\,erg^{-1}}.$$

As a result, $v_\lambda \approx 1.5 \times 10^9\,\mathrm{cm\,s^{-1}} \gg v_\mu$ and $v_\lambda \ll c_{\rm s} \approx 2 \times 10^{10}\,\mathrm{cm\,s^{-1}}$, so we are in regime I where turbulence develops. Finally, we estimate the length of the inertial range of chiral magnetically driven turbulence from

$$v_\mu / v_\lambda = \eta(\overline{\rho}\lambda)^{1/2} \approx g_{100}^{1/2}/2400. \tag{20}$$

Equation (13) with $\sqrt{C_\mu/C_\lambda} \approx 4$ gives $\mu/k_\lambda \approx 600 g_{100}^{-1/2}$. So

Inverse cascading

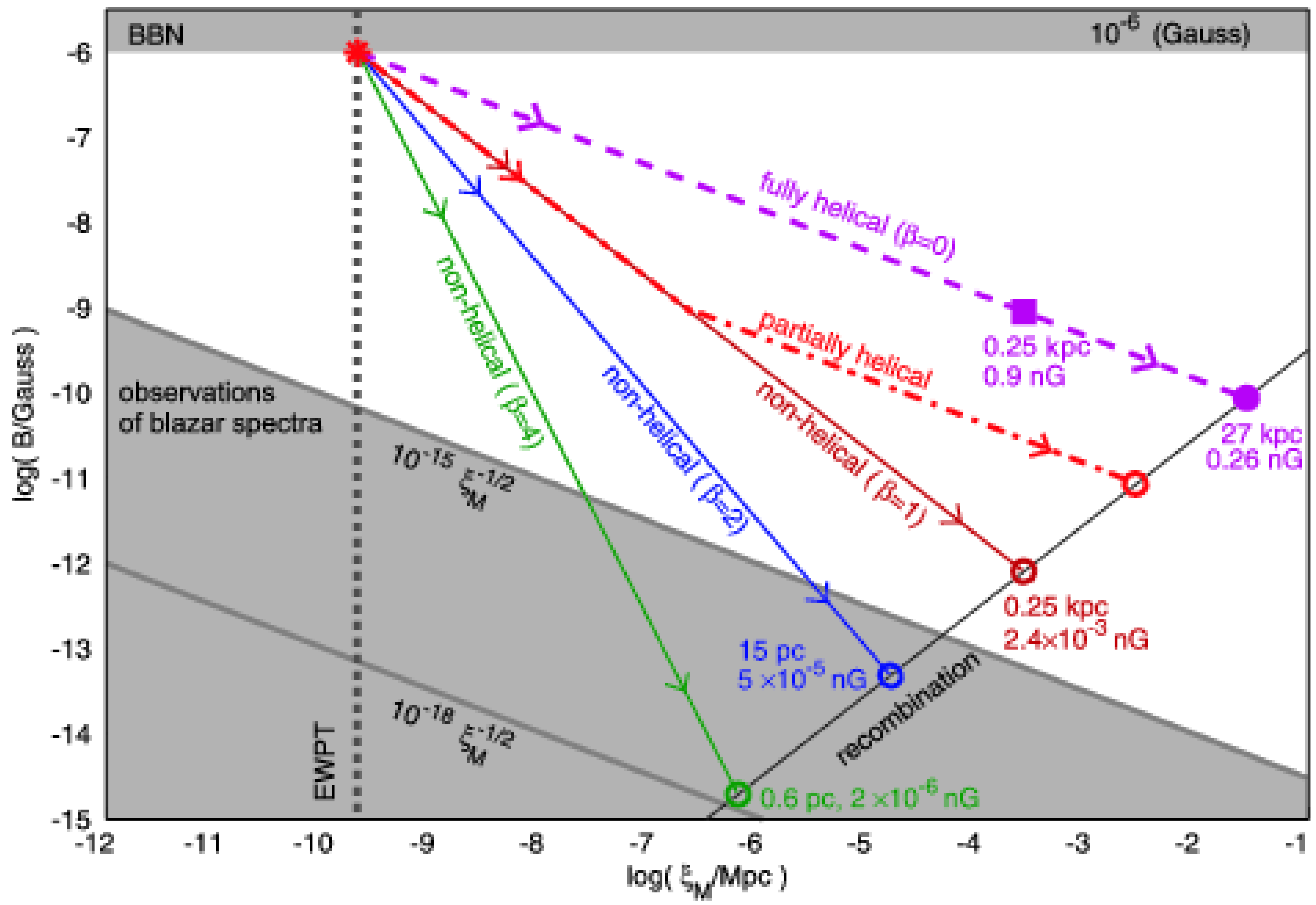

But initial length scale is very small

Starting point further to the left

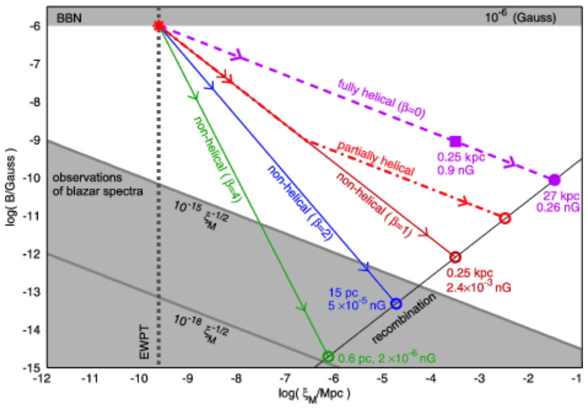

How to boost primordial helicity

Limit on magnetic energy can be much larger

$$\langle \boldsymbol{B}^2 \rangle / 2 \lesssim \epsilon_1 (k_{\rm B} T_0)^4 / (\hbar c)^3,$$

Problem: we need to constrain magnetic helicity

$$\langle \boldsymbol{B}^2 \rangle \xi_{\rm M} \lesssim \epsilon_2 (k_{\rm B} T_0)^3 / (\hbar c)^2,$$

Another possibility (e.g. if length scale = Hubble scale)

$$\langle \boldsymbol{B}^2 \rangle \xi_{\rm M} \lesssim \epsilon_3 (a_\star / a_0)^3 G^{-3/2} \hbar^{-1/2} c^{11/2},$$

e.g. if length scale = Hubble scale

$$\langle \boldsymbol{B}^2 \rangle \xi_{\rm M} \lesssim \epsilon_2^{2/3} \epsilon_3^{1/3} (a_\star / a_0) (k_{\rm B} T_0)^2 G^{-1/2} \hbar^{-3/2} c^{1/2},$$